Metal-like Electrical Conductance in Boron Fullerenes

Haiying He and Ravindra Pandey*

Department of Physics and Multi-scale Technology Institute, Michigan Technological University, Houghton, Michigan 49931

Ihsan Boustani

Fachbereich C- Theoretische Chemie, Universität Wuppertal, Gauss Str. 20, D-42097 Wuppertal, Germany

Shashi P. Karna*

US Army Research Laboratory, Weapons and Materials Research Directorate, ATTN: RDRL-WM, Aberdeen Proving Ground, Maryland 21005-5069

Received: October 6, 2009; Revised Manuscript Received: December 8, 2009

Electron transport properties of B-fullerenes, B_{80} and B_{100}, are investigated with the use of the first-principles density functional theory (DFT), in conjunction with the Landauer−Büttiker formalism and compared with C-fullerene, C_{60}, under similar conditions. The differential conductance and the tunnel current for B-fullerenes sandwiched between Au contacts are calculated to be much higher than those for C_{60}. An analysis of the calculated density of states and frontier orbitals suggests such a behavior of B-fullerenes to result from metal-like states, formed from the hybridization of Au 6s orbital with the highest occupied molecular orbital of B-fullerenes delocalized over the equator of the icosahedral cages, generally absent in Au−C_{60}−Au complex. Due to their enhanced electron transport properties, B-fullerenes appear to be attractive candidates for future nanoscale electronics.

I. Introduction

Boron nanostructures have been the subject of a number of recent theoretical[1−24] and experimental[25−38] studies. Theoretical studies have shown[1−6] that at low dimension, boron prefers to organize in planar or quasiplanar structures despite its preference for three-dimensional (3D) structural motifs in natural structures.[39] Theoretical studies predict B-nanostructures, such as two-dimensional (2D) boron sheet,[7−9] single-walled boron nanotubes (SWBNT),[10−16] bundles of SWBNTs,[17] and Mg-doped SWBNTs,[18] to be quite stable. An important feature of the B-nanostructures, as identified in the theoretical studies, is the presence of multicenter bonds, which play a prominent role in determining their stability and electron transport properties.

Boron structures also exhibit remarkable morphology-dependent electrical properties. For example, the three-dimensional (3D) boron crystalline solids[39] (e.g., α- and β-phases) and boron nanowires[25−38] are known to be semiconducting. In contrast, the two-dimensional (2D) B structures, such as B-sheets and their tubular forms, have been shown by first-principles calculations to exhibit remarkable metallic properties.[3,16] Thus, it seems that planar or quasiplanar confined boron coordination are a prerequisite for the predicted metallic behavior of B-nanostructures. One would, therefore, hypothesize that B_{80} and B_{100}, with 3D cage structures, would either exhibit a semiconducting behavior or an insulating behavior due to large gaps between the one-electron levels in the energy spectrum resulting from quantum confinement in a small space. To examine such a hypothesis and also to develop a fundamental understanding of the structure−electrical property relationship of B-nanostructures, we have investigated electron transport properties of the two B-icosahedral structures, B_{80} and B_{100}, with the use of the first-principles DFT in the framework of the Landauer−Büttiker formalism. Contrary to our expectations, both B-fullerene structures exhibit metallic character, similar to B-nanotube (BNT). The tunnel currents calculated as a function of applied external potential in the Au−B_{80}−Au and Au−B_{100}−Au architectures are considerably higher than that in the Au−C_{60}−Au system, with the larger B-fullerene (B_{100}) exhibiting an enhancement in the current by a factor of 4 over the smaller B-fullerene (B_{80}) and by a factor of 20 over the C-fullerene (C_{60}) at applied bias of 1.5 V.

B-fullerenes can be constructed from 2D boron sheets composed of triangular and hexagonal motifs.[19−24] In addition, the hexagon rings prefer to have an extra boron atom at the center, following the Aufbau principle. Similar to C-fullerenes, the B-fullerene structures are predicted to be more stable at certain "magic" numbers, such as B_{80}. Upon further increasing the number of B atoms in a hollow cluster, the spheroidal fullerene structure becomes energetically less favored than the tubular structure.[19]

The B_{80} molecule can be seen as a derivative of C_{60}-like structure by adding one extra atom at the center of each of the hexagons, which will be referred to as the "centered hexagons". Thus, it consists of 12 pentagons and 20 centered hexagons, resulting in an icosahedral, I_h, symmetry. The centered hexagons are cross-linked throughout the global molecule. Similarly, the B_{100} molecule can be derived from an icosahedral C_{80} structure by adding extra atoms at the center of 20 of its 30 hexagons, reducing the symmetry to D_{5d}. An interesting feature of the B-fullerene structures, B_{80} and B_{100}, is the formation of the linked B-centered hexagon belt at the equatorial position of

* To whom correspondence should be addressed. E-mail: pandey@mtu.edu (R.P), shashi.karna@us.army.mil (S.P.K.).

10.1021/jp9095776
Published on Web 02/10/2010

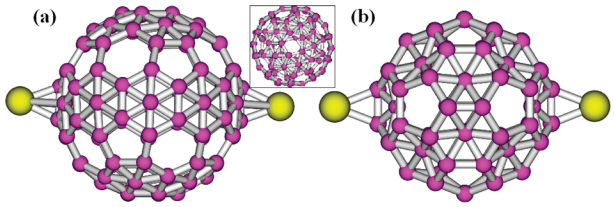

Figure 1. Schematic illustrations of the extended fullerene complexes, (a) B_{100} and (b) B_{80}. The inset shows a top view of B_{100}. The left/right contact region is modeled by gold atomic chain and the rest of the semi-infinite electrode is gold bulk reservoir, described by an effective self-energy, Σ.

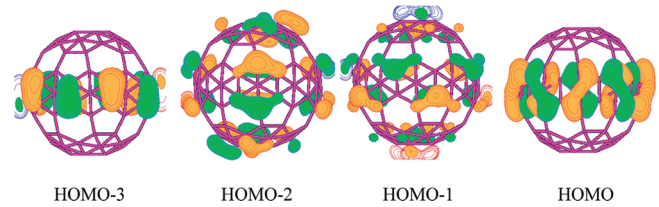

Figure 2. Plots of frontier orbitals of B_{100}. The so-called belt electronic states are located around the centered-hexagon belt at the celestial equator region of the fullerene configuration.

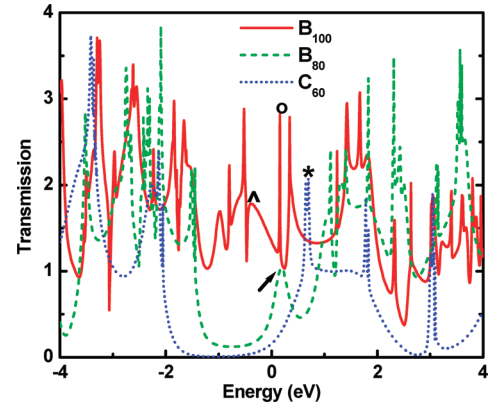

Figure 3. Transmission functions for B_{100}, B_{80}, and C_{60}. Zero of the energy is aligned to the pseudo-Fermi level. The labeling of some of the transmission peaks is discussed in the text.

the fullerene cages. This so-called "belt" structure is formed by properly selecting B-centered hexagons along the celestial equator, which are separated from other centered hexagons at the two polar caps (Figure 1). This feature, as will be shown in the later section, is found to play a critical role in the unique electronic and electron transport properties of B-fullerenes.

The wheel-like centered hexagons of B_{100} acquire a convex shape, while those of B_{80} are in the concave shape. Due to the difference in the inflection of the centered hexagons, B_{100} structure maintains a rather more smoother shape than B_{80}. We also find that B_{100} exhibits competitive energetic stability, as shown by B_{80}, although it does not belong to either the proposed stable families of $80n^2$ or $32 + 8n$ ($n > 0$).[19,20]

II. Computational Method

The symmetry-constrained geometry optimization calculations for B- and C-fullerenes were performed by the Gaussian 03 electronic structure suite of codes[40] together with the B3LYP functional[41,42] in the DFT and 6-31G* basis set. The optimized structures of B_{80}, B_{100}, and C_{60} compares well with the previously reported geometries.[21,22] For example, the calculated (average) bond length of the energy-optimized B_{80}, B_{100}, and C_{60} structures is found to be 1.66, 1.72, and 1.44 Å, respectively. At the B3LYP-DFT/6-31G* level, the binding energy of B_{100} is calculated to be slightly higher than that of B_{80}, suggesting the former to be energetically comparable to or more stable than the latter. The respective binding energies for B_{80}, B_{100}, and C_{60} are 5.16, 5.17, and 6.97 eV/atom. For B_{80}, the most stable isomer is predicted to have T_h symmetry, though the difference between the T_h and the I_h symmetry isomers is quite small, as also reported in a previous study.[19]

The electron transport calculations on the fullerenes coupled to semi-infinite Au electrodes (Figure 1) were performed following the Landauer−Büttiker formalism.[43−45] The core scattering region was simulated by the extended fullerene complex, Au−fullerene−Au, where atomic scale contacts were used for the fullerene molecule.

The total current in the Au−fullerene−Au system can be written as[45]

$$I = \frac{2e}{h}\int_{-\infty}^{\infty}\det(E,V)[f(E-\mu_1) - f(E-\mu_2)] \qquad (1)$$

In the above equation, μ_1 and μ_2 are the electrochemical potentials in the two contacts under an external bias V, $f(E)$ is the Fermi−Dirac distribution function, and $T(E,V)$ is the energy- and voltage-dependent transmission function, which can be calculated from a knowledge of the molecular energy levels and their coupling to the metallic contacts. In the scattering region, the bridge site between two six-member rings was taken to be the binding site of the metallic contact atom[3] with the Au−B and Au−C bond distances kept at 2.2 and 2.4 Å, respectively. Note that the contacts represented by a pyramidal Au_4 cluster with one Au atom protruding toward the fullerene molecule do not show a significant difference in the calculated transmission function, as also reported for the Al−C_{60}−Al system.[46] Additional details of the calculations can be found elsewhere.[47,48]

III. Results and Discussion: Electron Transport

Figure 2 shows selected occupied orbitals in the vicinity of the HOMO for B_{100}, which lie close in energy within 0.3 eV and are located around the centered-hexagon belt at the celestial equator region of the fullerene configuration. We call them the "belt" electronic states, in which the three-center bonds representing delocalized electronic density are prominent (Figure 2). These belt electronic states arrange slightly differently for each molecular orbital in boron fullerenes. Later, we will show that the existence of the belt states in the frontier orbitals is critical for the metal-like conduction of boron fullerenes.

The calculated transmission functions for B_{100}, B_{80}, and C_{60} are shown in Figure 3. The transmission function, in general, reflects the intrinsic transmission characteristics of a molecule and is related to the energy spectrum and the strength of coupling with the contact electrodes. A large HOMO−LUMO gap (~2.7 eV) of the C_{60} molecule reflects itself in a vanishing transmission in the near-Fermi region. The closest transmission peak at ~0.7 eV (labeled by an asterisk in Figure 3) is due to the LUMO-derived states, i.e., two C_{60}-LUMO states and one hybrid state of gold and C_{60}-LUMO (Please note that the isolated C_{60} molecule has three-fold degenerate LUMOs). These results are consistent with an earlier electron transport study on C_{60}.[49]

In contrast to C_{60}, both B_{80} and B_{100} have nonzero transmission at the zero injection energy. The diffusive transmission peaks in the near-Fermi region for B_{80} and B_{100} correspond to

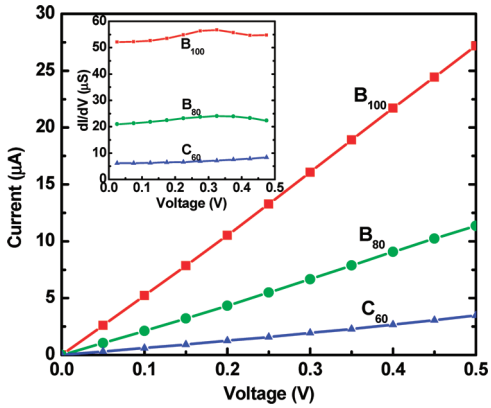

Figure 4. The current−voltage characteristics of the extended fullerene complex Au−fullerene−Au.

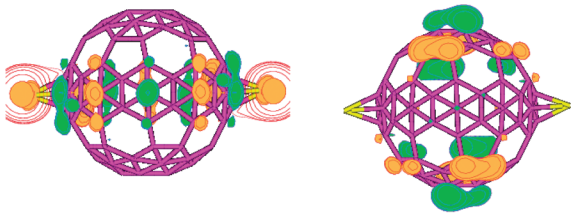

Figure 5. The frontier orbitals of the extended fullerene complex Au−B_{100}−Au. HOMO is a hybridized state derived from Au and B_{100}-belt states, while LUMO is derived only from B_{100}.

transmission via Au−B hybrid states. As one can expect from the transmission functions, the values of tunneling current (I) and differential conductance (dI/dV) for B_{80} and B_{100} are much higher than those for C_{60}, as shown in Figure 4.

The transmission gap, due to the HOMO−LUMO gap, is still tractable for B_{80}. Within the gap, there are two metal-induced gap (MIG) states resulting from the hybridization of Au 6s and B_{80} states, located mainly on the B−B bridge sites binding with the Au contacts. The wave function of these MIG states do not show any similarity with the isolated B_{80} molecular states near E_F. The HOMO state is rather delocalized, leading to a very diffusive transmission without showing a distinguishable peak. The LUMO state of the system, which is more localized at the Au-bonding region, accounts for the sharper transmission peak at ∼0.2 eV (labeled by an arrow in Figure 3) for B_{80}.

The charge transfer from Au to B_{80} is about the same as that from Au to C_{60}. Nonetheless, the magnitude of the transmission and current is much larger in the case of B_{100} and even nonvanishing through the whole energy region considered here from −4 to 4 eV. In other words, a HOMO−LUMO gap of ∼0.4 eV does not lead to a zero transmission region but rather a baseline of $\sim G_0$ (quantum conductance) in the transmission in B_{100}. Some of the frontier molecular orbitals in the near-Fermi region for the extended fullerene complex (i.e., Au−B_{100}−Au) are shown in Figure 5. The HOMO is again a hybrid of Au 6s and B_{100} states, which is an analogue of the HOMO of the isolated B_{100} fullerene with a shift of the electronic wave function from the hexagon edge to the hexagon center line along the belt. This HOMO state explains the nonzero transmission at the Fermi level for Au−B_{100}−Au. The hybridization of Au 6s and the isolated B_{100} HOMO state leads to a state about 1.07 eV lower in energy than the HOMO deep into the occupied states of the extended fullerene complex. The HOMO-1 state of the extended fullerene complex is a hybrid state of Au 5d orbital and B_{100} orbital states, where the electron

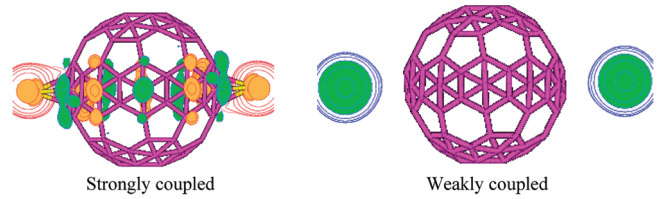

Figure 6. HOMO of the extended fullerene complex, Au−B_{100}−Au in the strongly coupled and weakly coupled (metal−molecule) regime.

distribution is rather localized, leading to a sharper peak (labeled by a caret in Figure 3). The LUMO and LUMO+1 states of the extended fullerene complex are molecular states corresponding to the 2-fold degenerate LUMOs of the isolated B_{100} molecule. These states generate a Fano resonance peak right above the Fermi level (labeled by an open circle in Figure 3). The charge transfer between Au and B_{100} is found to be negligibly small.

In order to understand the role of chemical bonding at the interface, calculations were also performed in the weakly coupled regime of the Au−B_{100}−Au system. The results show a small shift in the positions of sharp transmission peaks as we move from a strongly coupled (i.e., $R_{Au-B} = 2.2$ Å) to a weakly coupled regime (i.e., $R_{Au-B} = 3.9$ Å). The total energy of the weakly coupled Au−B_{100}−Au is about 2.5 eV higher than the strongly coupled Au−B_{100}−Au system.

The magnitude of transmission at the Fermi level decreases with an increase in the Au−fullerene distance and becomes negligible in a weakly coupled region where B_{100} has almost no bonding with Au. This can be directly attributed to the evolution of molecular orbitals at the interface as a function of the separation. For example, the HOMO state of the extended fullerene complex in the weakly coupled regime becomes a pure Au state relative to that in the strongly coupled regime, where it is a hybrid state with contributions from Au and B_{100} belt states (see Figure 6). Thus, the so-called "belt" electronic states, which are delocalized over the equator of the cages, appear to play a critical role on the metal-like conducting behavior of the B-fullerenes. Interestingly, the calculated metal-like conducting behavior of boron nanotubes[12] is also found to result from the presence of delocalized multicenter bonds in boron nanotubes. It is worth noting that theoretical calculations predict B-nanotubes to have a much higher conductivity than metallic carbon nanotubes.[12]

IV. Summary

The B-nanostructures possess unique chemical bonding and electronic properties. The presence of delocalized, multicenter bonds, with electron-deficient characteristics in the B-nanostructures, also yields novel electrical conducting properties. We show that B_{80} and B_{100} fullerene structures exhibit substantially enhanced electron transmission as well as tunneling currents compared to C_{60}. The B-fullerenes have nonvanishing transmission near E_F compared to a large transmission gap near E_F in the case of C_{60}. A highly pronounced transmission in the case of B_{100}, with a baseline of $\sim G_0$ over the whole energy range considered from −4 to 4 eV, shows the behavior of a metallic quantum contact.[50] The enhanced conducting feature of the B-fullerenes is closely related to their geometrical and electronic properties, which are characterized by a series of "belt states" at the celestial equator. Hybridization of these belt or belt-derived states with the Au 6s and/or 5d states results in high electron transmission baseline. The decoupling of the Au

electrode and B_{100}, however, closes the electron transport channels due to these states, making several transmission gaps shown over the energy considered. Thus, similar to B-nanotubes, the presence of delocalized multicenter bonds and their coupling/hybridization with the metal (Au) states appear to lead to the metal-like conducting properties of B-fullerenes. These unique chemical bonding features of B-nanostructures can be useful in the development of future molecular or hybrid molecular electronics.

Acknowledgment. The work at Michigan Technological University was performed under support by Army Research Office through contract number W911NF-09-1-0221 and Army Research Laboratory through contract number W911NF-09-2-0026.

References and Notes

(1) Derecskei, A.; Dunlap, B. I.; Lipscomb, W. N.; Lowrey, A.; Marynick, D. S.; Massa, L. *Inorg. Chem.* **1994**, *33*, 5617.
(2) Boustani, I. *Phys. Rev. B* **1997**, *55*, 16426. Boustani, I. *Solid State Chem.* **1997**, *133*, 182.
(3) Lau, K. C.; Pandey, R. *CoLe* **2005**, *1*, 1.
(4) Lau, K. C.; Deshpande, M. D.; Pati, R.; Pandey, R. *Int. J. Quantum Chem.* **2005**, *103*, 866.
(5) Lau, K. C.; Deshpande, M. D.; Pandey, R. *Int. J. Quantum Chem.* **2005**, *102*, 656.
(6) Alexandrova, A. N.; Boldyrev, A. I.; Zhai, H.; Wang, L. *Coord. Chem. Rev.* **2006**, *250*, 2811.
(7) Evans, M. H.; Joannopoulos, J. D.; Pantelides, S. T. *Phys. Rev. B* **2005**, *72*, 045434.
(8) Kunstmann, J.; Quandt, A. *Phys. Rev. B* **2006**, *74*, 035413.
(9) Lau, K. C.; Pandey, R. *J. Phys. Chem. C* **2007**, *111*, 2906.
(10) Quandt, A.; Boustani, I. *ChemPhysChem* **2005**, *6*, 2001, and references therein.
(11) Lau, K. C.; Pati, R.; Pandey, R.; Pineda, A. C. *Chem. Phys. Lett.* **2006**, *418*, 549.
(12) Lau, K. C.; Pandey, R.; Pati, R.; Karna, S. P. *Appl. Phys. Lett.* **2006**, *88*, 212111.
(13) Tang, H.; Ismail-Beigi, S. *Phys. Rev. Lett.* **2007**, *99*, 115501.
(14) Yang, X.; Ding, Y.; Ni, J. *Phys. Rev. B.* **2008**, *77*, 041402®.
(15) Singh, A. K.; Sadrzadeh, A.; Yokobson, B. I. *Nano Lett.* **2008**, *8*, 1314.
(16) Lau K. C. Pandey R. *Boron and Boron Carbide Materials: Nanostructures and Crystalline Solids. Lecture Notes in Nanoscale Science and Technology*; Springer: New York, 2009.
(17) Lau, K. C.; Orlando, R.; Pandey, R. *J. Phys: Condens. Matter* **2008**, *20*, 125202.
(18) Lau, K. C.; Orlando, R.; Pandey, R. *J. Phys: Condens. Matter* **2009**, *21*, 45304.
(19) Zope, R. R.; Baruah, T.; Lau, K. C.; Liu, A. Y.; Pederson, M. R.; Dunlap, B. I. *Phys. Rev. B* **2009**, *79*, 161403(R).
(20) Yan, Q.-B.; Sheng, X.-L.; Zheng, Q. -R.; Zhang, L.-Z.; Su, G. *Phys Rev B* **2008**, *78*, 201401.
(21) Prasad, D. L. V.; Jemmis, E. D. *Phys. Rev. Lett.* **2008**, *100*, 165504.
(22) Szwacki, N. G. *Nanoscale Res. Lett.* **2008**, *100*, 165504.
(23) Szwacki, N. G.; Sadrzadeh, A.; Yakobson, B. I. *Phys. Rev. Lett.* **2007**, *98*, 166804.
(24) Botti, S.; Castro, A.; Nektraios, N. N.; Andrade, X.; Marques, M. A. L. *Phys. Chem. Chem. Phys.* **2009**, *11*, 4523.
(25) Wu, Y. Y.; Messer, B.; Yang, P. D. *Adv. Mater. (Weinheim, Ger.)* **2001**, *13*, 1487.
(26) Cao, L.; et al. *J. Phys.: Condens. Matter* **2002**, *14*, 11017.
(27) Wang, Q. Y.; Duan, X. F. *Appl. Phys. Lett.* **2003**, *82*, 272.
(28) Otten, C. J.; Lourie, O. R.; Yu, M. F.; Cowley, J. M.; Dyer, M. J.; Ruoff, R. S.; Buhro, W. E. *J. Am. Chem. Soc.* **2002**, *124*, 4564.
(29) Meng, X. M.; Hu, J. Q.; Jiang, Y.; Lee, C. S.; Lee, S. T. *Chem. Phys. Lett.* **2003**, *370*, 825.
(30) Wang, D. W.; Lu, J. G.; Otten, C. J.; Buhro, W. E. *Appl. Phys. Lett.* **2003**, *83*, 5280.
(31) Wang, Z. K.; Shimizu, Y.; Sasaki, T.; Kawaguchi, K.; Kimura, K.; Koshizaki, N. *Chem. Phys. Lett.* **2003**, *368*, 663.
(32) Yun, S. H.; Dibos, A.; Wu, J. Z.; Kim, D. K. *Appl. Phys. Lett.* **2004**, *84*, 2892.
(33) Xu, T. T.; Zheng, J. G.; Wu, N. Q.; Nicholls, A. W.; Roth, J. R. D.; Dikin, A.; Ruoff, R. S. *Nano Lett.* **2004**, *4*, 963.
(34) Yun, S. H.; Wu, J. Z.; Dibos, A.; Zou, X.; Karlsson, U. O. *Nano Lett.* **2006**, *6*, 385.
(35) Yun, S. H.; Dibos, A.; Lee, H. S.; Wu, J. Z.; Karlsson, U. O. *Appl. Surf. Sci.* **2006**, *252*, 5587.
(36) Guo, L.; Singh, R. N.; Kleebe, H.-J. *Chem. Vapor Deposit.* **2006**, *12*, 448–452. Guo, L.; Singh, R. N.; Kleebe, H.-J. *J. Nanomater.* **2006**, 1.
(37) Wang, X. J.; Tian, J. F.; Yang, T. Z.; Bao, L. H.; Hui, C.; Liu, F.; Shen, C. M.; Gu, C. Z.; Xu, N. S.; Gao, H. J. *Adv. Mater. (Weinheim, Ger.)* **2007**, *19*, 4480.
(38) Tian, J.; Cai, J.; Hui, C.; Zhang, C.; Bao, L.; Gao, M.; Shen, C.; Gao, H. *Appl. Phys. Lett.* **2008**, *93*, 122105.
(39) Muetterties E. L. (Ed.) *The Chemistry of Boron and its Compounds*; John Wiley: New York, 1967.
(40) Frisch M. J. Gaussian 03, Gaussian, Inc.: Pittsburgh PA, 2003.
(41) Becke, A. D. *J. Chem. Phys.* **1993**, *98*, 5648.
(42) Lee, C.; Yang, W.; Parr, R. G. *Phys. Rev. B* **1998**, *37*, 785.
(43) Landauer, R. *J. Phys.: Condens. Matter* **1989**, *1*, 8099.
(44) Büttiker, M. *Phys. Rev. Lett.* **1986**, *57*, 1761.
(45) Datta S. *Electronic Transport Properties in Mesoscopic Systems*; Cambridge University Press: Cambridge, 1995.
(46) Palacios, J. J.; Pérez-Jiménez, A. J.; Louis, E.; Vergés, J. A. *Phys. Rev. B* **2001**, *64*, 115411.
(47) Tian, W.; Datta, S.; Hong, S.; Reifenberger, R.; Henderson, J. I.; Kubiak, C. P. *J. Chem. Phys.* **1998**, *109*, 2874.
(48) He, H.; Pandey, R.; Karna, S. P. *Chem. Phys. Lett.* **2007**, *439*, 110.
(49) Sergueev N., Roubtsov D. Guo H. arXiv:cond-mat/0309614v1 [cond-mat.mtrl-sci].
(50) Garcia-Suarez, V.; Rocha, A. R.; Bailey, S. W.; Lambert, C. J.; Sanvito, S.; Ferrer, J. *Phys. Rev. Lett.* **2005**, *95*, 256804, and references therein.

JP9095776